Ch. 6

General comment
bigger letters and formulae

cf. comment p. 21

like original notes on Knock out

Chapter 6

One–particle transfer

In what follows we present a derivation of the one–particle transfer differential cross section within the framework of ~~the~~ (DWBA) cf. Satchler (1980); Broglia and Winther (2004) and refs. therein). The structure input for the calculations are mean field potentials and single–particle states dressed through the coupling with the variety of collective, (quasi) bosonic vibrations, leading to modified formfactors[1] resulting ~~from~~ the interweaving of these vibrations and a number of ~~orbitals with the~~ original, unperturbed single–particle state (Bohr and Mottelson, 1975; Bès and Broglia, 1977). With the help of these modified formfactors, and of optical potentials, one can calculate the absolute differential cross sections, quantities which can be directly compared with the experimental findings.

In this way one avoids to introduce, let alone use spectroscopic factors, quantities which are rather elusive to define. This is in keeping with the fact that as a nucleon moves through the nucleus it feels the presence of the other nucleons whose configurations change as time proceeds. It takes time for this information to be fed back on the nucleon. This renders the average potential nonlocal in time (cf. C. Mahaux et al. (1985) and references therein). A time–dependent operator can always be transformed into an energy dependent operator, implying an ω–dependence of the properties which are usually adscribed to particles like (effective) mass, charge, etc. Furthermore, due to ~~the~~ Pauli principle, the average potential is also non local in space (cf. Apps 6.A and 6.B) Consequently, one is forced to deal with nucleons which carry around a cloud of (quasi) bosons, aside from exchanging its position with that of the other nucleons. It is of notice that the above mentioned phenomena are not only found ~~within the realm of~~ nuclear physics, but are common within the framework of many–body systems as well as of field theories like quantum electrodynamic (QED). In fact, a basic result of such theories is that nothing is really free (Feynman, 1975). A textbook example being provided by the Lamb shift, resulting from the dressing of the hydrogen atom electron, as a result of the exchange of this electron with those participating in the spontaneous, virtual excitation (zero point fluctuations (ZPF)) of the QED vacuum (cf. Apps 6.C and 6.D). Within this context see Sect. 6.2 (Examples and Applications) concerning the phenomenon of parity inversion in the N=6 (closed shell) of exotic halo nuclei.

[1] It is of notice that single–particle modified formfactors have their counterpart in the renormalised transition densities (Ch. 5 (inelastic scattering)) and in the modified two–nucleon transfer formfactors (Chapter ~~7.2.10 and 8.2.3~~) associated with inelastic and with pair transfer (Broglia et al., 1973) reactions, respectively.

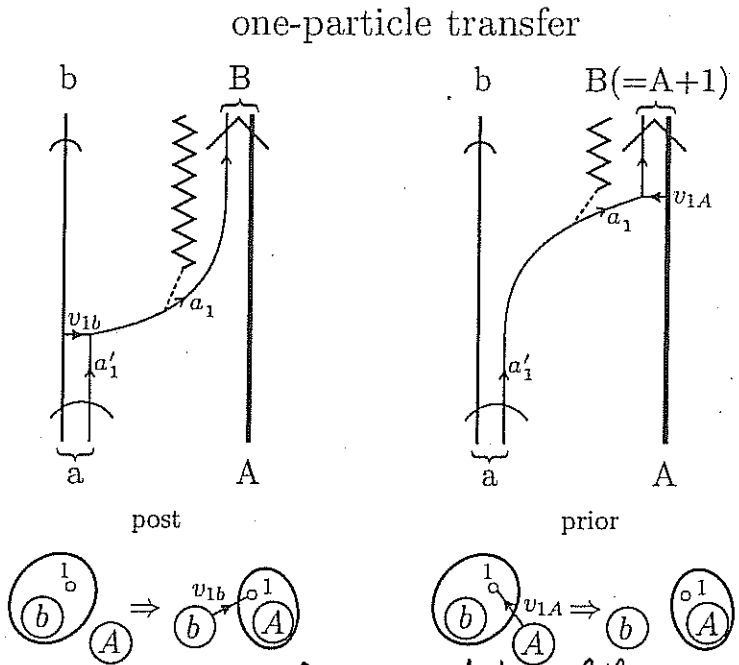

Figure 6.1.1: One–particle reaction $a(= b + 1) + A \rightarrow b + B(= A + 1)$. The time arrow is assumed to point upwards. The quantum numbers characterizing the states in which the transferred nucleon moves in projectile and target are denoted a'_1 and a_1 respectively. The interaction inducing the nucleon to be transferred can act either in the entrance channel ((a, A); v_{1A}, prior representation) or in the exit channel ((b, B); v_{1b}, post representation), in keeping with energy conservation. In the transfer process, the nucleon changes orbital at the same time that a change in the mass partition takes place. The corresponding relative motion mismatch is known as the recoil process, and is represented by a jagged line which provides information on the evolution of r_{1A} (r_{1b}). In other words, on the coupling of reaction and transfer modes.

6.1 General derivation

We proceed now to derive the transition amplitude for the reaction (cf. Fig. 6.1.1). For a simplified version we refer to App 6.E, while for an alternative derivation within the framework of knock–out reactions cf. App 6.F.

$$A + a(= b + 1) \longrightarrow B(= A + 1) + b. \qquad (6.1.1)$$

Let us assume that the nucleon bound initially to the core b is in a single–particle state with orbital and total angular momentum l_i and j_i respectively, and that the nucleon in the final state (bound to core A) is in the l_f, j_f state. The total spin and magnetic quantum numbers of nuclei A, a, B, b are $\{J_A, M_A\}, \{J_a, M_a\}, \{J_B, M_B\}, \{J_b, M_b\}$ respectively. Denoting ξ_A and ξ_b the intrinsic coordinates of the wavefunctions describing the structure of nuclei A and b respectively, and $\mathbf{r}_{An}$ and $\mathbf{r}_{bn}$ the relative coordinates of the transferred nucleon with respect to the CM of nuclei A and b respectively, one can

write the "intrinsic" wavefunctions of the colliding nuclei A, a as

$$\phi^{J_A}_{M_A}(\xi_A),$$
$$\Psi(\xi_b, \mathbf{r}_{bt}) = \sum_{m_i} \langle J_b\ j_i\ M_b\ m_i | J_a\ M_a\rangle \phi^{J_b}_{M_b}(\xi_b)\psi^{j_i}_{m_i}(\mathbf{r}_{bn}, \sigma), \tag{6.1.2}$$

while the "intrinsic" wavefunctions describing the structure of nuclei B and b are

$$\phi^{J_b}_{M_b}(\xi_b),$$
$$\Psi(\xi_A, \mathbf{r}_{At}) = \sum_{m_f} \langle J_A\ j_f\ M_A\ m_f | J_B\ M_B\rangle \phi^{J_A}_{M_A}(\xi_A)\psi^{j_f}_{m_f}(\mathbf{r}_{An}, \sigma). \tag{6.1.3}$$

For an unpolarized incident beam (sum over M_A, M_a and divide by $(2J_A+1), (2J_a+1)$), and assuming that one does not detect the final polarization (sum over M_B, M_b), the differential cross section in the DWBA can be written as

$$\frac{d\sigma}{d\Omega} = \frac{k_f}{k_i}\frac{\mu_i\mu_f}{4\pi^2\hbar^4}\frac{1}{(2J_A+1)(2J_a+1)} \times \sum_{\substack{M_A,M_a\\M_B,M_b}} \left| \sum_{m_i,m_f} \langle J_b\ j_i\ M_b\ m_i | J_a\ M_a\rangle \langle J_A\ j_f\ M_A\ m_f | J_B\ M_B\rangle T_{m_i,m_f} \right|^2, \tag{6.1.4}$$

The transition amplitude T_{m_i,m_f} is

$$T_{m_i,m_f} = \sum_{\sigma} \int d\mathbf{r}_f d\mathbf{r}_{bn} \chi^{(-)*}(\mathbf{r}_f)\psi^{j_f*}_{m_f}(\mathbf{r}_{An}, \sigma)V(r_{bn})\psi^{j_i}_{m_i}(\mathbf{r}_{bn}, \sigma)\chi^{(+)}(\mathbf{r}_i), \tag{6.1.5}$$

where

$$\psi^{j_i}_{m_i}(\mathbf{r}_{An}, \sigma) = u_{j_i}(r_{bn})\left[Y^{l_i}(\hat{r}_i)\chi(\sigma)\right]_{j_i m_i}, \tag{6.1.6}$$

is the single–particle wavefunction describing the motion of the nucleon to be transferred, when in the initial state. Similarly for $\psi^{j_f}_{m_f}$. The ~~incoming and outgoing~~ distorted waves are

$$\chi^{(+)}(\mathbf{k}_i, \mathbf{r}_i) = \frac{4\pi}{k_i r_i}\sum_{l'} i^{l'} e^{i\sigma_{l'}} g_{l'}(\hat{r}_i)\left[Y^{l'}(\hat{r}_i)Y^{l'}(\hat{k}_i)\right]^0_0, \tag{6.1.7}$$

and

$$\chi^{(-)*}(\mathbf{k}_f, \mathbf{r}_f) = \frac{4\pi}{k_f r_f}\sum_{l} i^{-l} e^{i\sigma_l} f_l(\hat{r}_f)\left[Y^{l}(\hat{r}_f)Y^{l}(\hat{k}_f)\right]^0_0, \tag{6.1.8}$$

respectively. ~~Now~~,

$$\left[Y^{l}(\hat{r}_f)Y^{l}(\hat{k}_f)\right]^0_0\left[Y^{l'}(\hat{r}_i)Y^{l'}(\hat{k}_i)\right]^0_0 = \sum_K ((ll)_0(l'l')_0|(ll')_K(ll')_K)_0 \times \left\{\left[Y^{l}(\hat{r}_f)Y^{l'}(\hat{r}_i)\right]^K\left[Y^{l}(\hat{k}_f)Y^{l'}(\hat{k}_i)\right]^K\right\}^0_0. \tag{6.1.9}$$

The $9j$–symbol can be explicitly evaluated to give,

$$((ll)_0(l'l')_0|(ll')_K(ll')_K)_0 = \sqrt{\frac{2K+1}{(2l+1)(2l'+1)}}, \tag{6.1.10}$$

while the coupled expression can be written as

$$\left\{ \left[Y^l(\hat{r}_f)Y^{l'}(\hat{r}_i)\right]^K \left[Y^l(\hat{k}_f)Y^{l'}(\hat{k}_i)\right]^K \right\}_0^0 = \sum_M \langle K\ K\ M\ -M|0\ 0\rangle \left[Y^l(\hat{r}_f)Y^{l'}(\hat{r}_i)\right]_M^K \times \left[Y^l(\hat{k}_f)Y^{l'}(\hat{k}_i)\right]_{-M}^K = \sum_M \frac{(-1)^{K+M}}{\sqrt{2K+1}} \left[Y^l(\hat{r}_f)Y^{l'}(\hat{r}_i)\right]_M^K \left[Y^l(\hat{k}_f)Y^{l'}(\hat{k}_i)\right]_{-M}^K . \tag{6.1.11}$$

Thus,

$$\left[Y^l(\hat{r}_f)Y^l(\hat{k}_f)\right]_0^0 \left[Y^{l'}(\hat{r}_i)Y^{l'}(\hat{k}_i)\right]_0^0 = \sum_{K,M} \frac{(-1)^{K+M}}{\sqrt{(2l+1)(2l'+1)}} \left[Y^l(\hat{r}_f)Y^{l'}(\hat{r}_i)\right]_M^K \left[Y^l(\hat{k}_f)Y^{l'}(\hat{k}_i)\right]_{-M}^K . \tag{6.1.12}$$

For the angular integral to be different from zero, the integrand must be coupled to zero angular momentum (scalar). Noting that the only variables over which one integrates in the above expression are $\hat{r}_i, \hat{r}_f$, we have to couple the remaining functions of the angular variables, namely the wavefunctions $\psi^{j_f*}_{m_f}(\mathbf{r}_{An}, \sigma) = (-1)^{j_f-m_f}\psi^{j_f}_{-m_f}(\mathbf{r}_{An}, -\sigma)$ and $\psi^{j_i}_{m_i}(\mathbf{r}_{bn}, \sigma)$ to angular momentum K, as well as to fulfill $M = m_f - m_i$. Let us then consider

$$(-1)^{j_f-m_f}\psi^{j_f}_{-m_f}(\mathbf{r}_{An}, -\sigma)\psi^{j_i}_{m_i}(\mathbf{r}_{bn}, \sigma) = (-1)^{j_f-m_f}u_{j_f}(r_{An})u_{j_i}(r_{bn}) \times \sum_P \langle j_f\ j_i\ -m_f\ m_i|P\ m_i - m_f\rangle \left\{ \left[Y^{l_f}(\hat{r}_{An})\chi^{1/2}(-\sigma)\right]^{j_f} \left[Y^{l_i}(\hat{r}_{bn})\chi^{1/2}(\sigma)\right]^{j_i} \right\}_{m_i-m_f}^P . \tag{6.1.13}$$

Recoupling the spherical harmonics to angular momentum K and the spinors to $S = 0$, only one term survives the angular integral in (6.1.5), namely

$$(-1)^{j_f-m_f}u_{j_f}(r_{An})u_{j_i}(r_{bn})((l_f\tfrac{1}{2})_{j_f}(l_i\tfrac{1}{2})_{j_i}|(l_fl_i)_K(\tfrac{1}{2}\tfrac{1}{2})_0)_K \times \langle j_f\ j_i\ -m_f\ m_i|K\ m_i - m_f\rangle \left[Y^{l_f}(\hat{r}_{An})Y^{l_i}(\hat{r}_{bn})\right]_{m_i-m_f}^K \left[\chi(-\sigma)\chi(\sigma)\right]_0^0 . \tag{6.1.14}$$

Making use of the fact that the sum over spins yields a factor $-\sqrt{2}$, and in keeping with the fact that $M = m_f - m_i$, one obtains,

$$T_{m_i,m_f} = (-1)^{j_f-m_f}\frac{-16\sqrt{2}\pi^2}{k_fk_i}\sum_{ll'} i^{l'-l}e^{\sigma_f^l+\sigma_i^{l'}} \sum_K ((l_f\tfrac{1}{2})_{j_f}(l_i\tfrac{1}{2})_{j_i}|(l_fl_i)_K(\tfrac{1}{2}\tfrac{1}{2})_0)_K \times \langle j_f\ j_i\ -m_f\ m_i|K\ m_i - m_f\rangle \left[Y^l(\hat{k}_f)Y^{l'}(\hat{k}_i)\right]_{m_i-m_f}^K \int d\mathbf{r}_f d\mathbf{r}_{bn} \frac{f_l(r_f)g_{l'}(r_i)}{r_fr_i} \times u_{j_f}(r_{An})u_{j_i}(r_{bn})V(r_{bn})(-1)^{K+m_f-m_i} \left[Y^l(\hat{r}_f)Y^{l'}(\hat{r}_i)\right]_{m_f-m_i}^K \left[Y^{l_f}(\hat{r}_{An})Y^{l_i}(\hat{r}_{bn})\right]_{m_i-m_f}^K . \tag{6.1.15}$$

Again, the only term of the expression

$$(-1)^{K+m_f-m_i}\left[Y^l(\hat{r}_f)Y^{l'}(\hat{r}_i)\right]_{m_f-m_i}^K \left[Y^{l_f}(\hat{r}_{An})Y^{l_i}(\hat{r}_{bn})\right]_{m_i-m_f}^K = (-1)^{K+m_f-m_i}\sum_P \langle K\ K\ m_f - m_i\ m_i - m_f|P\ 0\rangle \left\{ \left[Y^l(\hat{r}_f)Y^{l'}(\hat{r}_i)\right]^K \left[Y^{l_f}(\hat{r}_{An})Y^{l_i}(\hat{r}_{bn})\right]^K \right\}_0^P$$

which survives after angular integration is the one with $P = 0$, that is,

$$\frac{1}{\sqrt{(2K+1)}}\left\{\left[Y^l(\hat{r}_f)Y^{l'}(\hat{r}_i)\right]^K\left[Y^{l_f}(\hat{r}_{An})Y^{l_i}(\hat{r}_{bn})\right]^K\right\}_0^0 =$$

$$\frac{1}{\sqrt{(2K+1)}}\sum_{M_K}\langle K\ K\ M_K\ -M_K|0\ 0\rangle\left[Y^l(\hat{r}_f)Y^{l'}(\hat{r}_i)\right]^K_{M_K}$$

$$\times\left[Y^{l_f}(\hat{r}_{An})Y^{l_i}(\hat{r}_{bn})\right]^K_{-M_K} = \frac{1}{\sqrt{(2K+1)}}\sum_{M_K}\frac{(-1)^{K+M_K}}{\sqrt{(2K+1)}}\left[Y^l(\hat{r}_f)Y^{l'}(\hat{r}_i)\right]^K_{M_K}$$

$$\times\left[Y^{l_f}(\hat{r}_{An})Y^{l_i}(\hat{r}_{bn})\right]^K_{-M_K} =$$

6.1.2

$$\frac{1}{2K+1}\sum_{M_K}(-1)^{K+M_K}\left[Y^l(\hat{r}_f)Y^{l'}(\hat{r}_i)\right]^K_{M_K}\left[Y^{l_f}(\hat{r}_{An})Y^{l_i}(\hat{r}_{bn})\right]^K_{-M_K},$$

an expression which is spherically symmetric. One can evaluate it for a particular configuration, in particular setting $\hat{r}_f = \hat{z}$ and the center of mass A, b, n in the $x-z$ plane (see Fig. 7.1). Once the orientation in space of this "standard" configuration is specified (through, for example, a rotation $0 \le \alpha \le 2\pi$ around $\hat{z}$, a rotation $0 \le \beta \le \pi$ around the new x axis and a rotation $0 \le \gamma \le 2\pi$ around $\hat{r}_{bB}$), the only remaining angular coordinate is θ, while the integral over the other three angles yields a $8\pi^2$. Setting $\hat{r}_f = \hat{z}$ one obtains

$$\left[Y^l(\hat{r}_f)Y^{l'}(\hat{r}_i)\right]^K_{M_K} = \langle l\ l'\ 0\ M_K|K\ M_K\rangle\sqrt{\frac{2l+1}{4\pi}}Y^{l'}_{M_K}(\hat{r}_i). \tag{6.1.16}$$

Because of $M = m_i - m_f$, and $m = m_f$, $T_{m_i,m_f} \equiv T_{m,M}$ where

$$T_{m,M} = (-1)^{j_f-m}\frac{-64\sqrt{2}\pi^{7/2}}{k_f k_i}\sum_{ll'}i^{l'-l}e^{\sigma_f^l+\sigma_i^{l'}}\sqrt{2l+1}\sum_K\frac{(-1)^K}{2K+1}((l_f\tfrac{1}{2})_{j_f}(l_i\tfrac{1}{2})_{j_i}|(l_f l_i)_K(\tfrac{1}{2}\tfrac{1}{2})_0)_K$$

$$\times\langle j_f\ j_i\ -m\ M+m|K\ M\rangle\left[Y^l(\hat{k}_f)Y^{l'}(\hat{k}_i)\right]^K_M\int d\mathbf{r}_f d\mathbf{r}_{bn}\frac{f_l(r_f)g_{l'}(r_i)}{r_f r_i}$$

$$\times u_{j_f}(r_{An})u_{j_i}(r_{bn})V(r_{bn})\sum_{M_K}(-1)^{M_K}\langle l\ l'\ 0\ M_K|K\ M_K\rangle\left[Y^{l_f}(\hat{r}_{An})Y^{l_i}(\hat{r}_{bn})\right]^K_{-M_K}Y^{l'}_{M_K}(\hat{r}_i). \tag{6.1.17}$$

We now turn our attention to the sum

$$\sum_{\substack{M_A,M_a\\M_B,M_b}}\left|\sum_{m,M}\langle J_b\ j_i\ M_b\ m|J_a\ M_a\rangle\langle J_A\ j_f\ M_A\ M-m|J_B\ M_B\rangle T_{m,M}\right|^2, \tag{6.1.18}$$

appearing in the expression for the differential cross section (6.1.4). For any given value m', M' of m, M, the sum will be

$$\sum_{M_a,M_b}|\langle J_b\ j_i\ M_b\ m'|J_a\ M_a\rangle|^2\sum_{M_A,M_B}\left|\langle J_A\ j_f\ M_A\ M'-m'|J_B\ M_B\rangle\right|^2\left|T_{m',M'}\right|^2$$

$$= \frac{(2J_a+1)(2J_B+1)}{(2j_i+1)(2j_f+1)}\sum_{M_a,M_b}|\langle J_b\ J_a\ M_b\ -M_a|j_i\ m'\rangle|^2$$

$$\times\sum_{M_A,M_B}\left|\langle J_A\ J_B\ M_A\ -M_B|j_f\ M'-m'\rangle\right|^2\left|T_{m',M'}\right|^2, \tag{6.1.19}$$

by virtue of the symmetry property of Clebsch–Gordan coefficients

$$\langle J_b\ j_i\ M_b\ m|J_a\ M_a\rangle = (-1)^{J_b-M_b}\sqrt{\frac{(2J_a+1)}{(2j_i+1)}}\langle J_b\ J_a\ M_b\ -M_a|j_i\ m\rangle. \qquad (6.1.20)$$

The sum over the Clebsch–Gordan coefficients in (6.1.19)is, so (6.1.18) is just

$$\frac{(2J_a+1)(2J_B+1)}{(2j_i+1)(2j_f+1)}\sum_{m,M}\left|T_{m,M}\right|^2, \qquad (6.1.21)$$

and the differential cross section turns out to be

$$\frac{d\sigma}{d\Omega} = \frac{k_f}{k_i}\frac{\mu_i\mu_f}{4\pi^2\hbar^4}\frac{(2J_B+1)}{(2j_i+1)(2j_f+1)(2J_A+1)}\sum_{m,M}\left|T_{m,M}\right|^2. \qquad (6.1.22)$$

where

$$T_{m,M} = \sum_{Kll'}(-1)^{-m}\langle j_f\ j_i\ -m\ M+m|K\ M\rangle\left[Y^l(\hat{k}_f)Y^{l'}(\hat{k}_i)\right]^K_M t^K_{ll'}. \qquad (6.1.23)$$

Orienting $\hat{k}_i$ along the incident z direction leads to,

$$\left[Y^l(\hat{k}_f)Y^{l'}(\hat{k}_i)\right]^K_M = \langle l\ l'\ M\ 0|K\ M\rangle\sqrt{\frac{2l'+1}{4\pi}}Y^l_M(\hat{k}_f), \qquad (6.1.24)$$

and

$$T_{m,M} = \sum_{Kll'}(-1)^{-m}\langle l\ l'\ M\ 0|K\ M\rangle\langle j_f\ j_i\ -m\ M+m|K\ M\rangle Y^l_M(\hat{k}_f)\,t^K_{ll'}, \qquad (6.1.25)$$

with

$$t^K_{ll'} = (-1)^{K+j_f}\frac{-32\sqrt{2}\pi^3}{k_fk_i}i^{l'-l}e^{\sigma^l_f+\sigma^{l'}_i}\frac{\sqrt{(2l+1)(2l'+1)}}{2K+1}((l_f\tfrac{1}{2})_{j_f}(l_i\tfrac{1}{2})_{j_i}|(l_fl_i)_K(\tfrac{1}{2}\tfrac{1}{2})_0)_K$$
$$\times\int dr_f\,dr_{bn}d\theta r^2_{bn}\sin\theta\, r_f\frac{f_i(r_f)g_{l'}(r_i)}{r_i}u_{j_f}(r_{An})u_{j_i}(r_{bn})V(r_{bn})$$
$$\times\sum_{M_K}(-1)^{M_K}\langle l\ l'\ 0\ M_K|K\ M_K\rangle\left[Y^{l_f}(\hat{r}_{An})Y^{l_i}(\hat{r}_{bn})\right]^K_{-M_K}Y^{l'}_{M_K}(\hat{r}_i). \qquad (6.1.26)$$

6.1.1 Coordinates

To perform the integral in (6.1.26), one needs the expression of $r_i, r_{An}, \hat{r}_{An}, \hat{r}_{bn}, \hat{r}_i$ in term of the integration variables r_f, r_{bn}, θ. Because one is interested in evaluating these quantities in the particular configuration depicted in Fig. 3.3.1, one has

$$\mathbf{r}_f = r_f\,\hat{z}, \qquad (6.1.27)$$
$$\mathbf{r}_{bn} = -r_{bn}(\sin\theta\,\hat{x}+\cos\theta\,\hat{z}), \qquad (6.1.28)$$
$$\mathbf{r}_{Bn} = \mathbf{r}_f+\mathbf{r}_{bn} = -r_{bn}\sin\theta\,\hat{x}+(r_f-r_{bn}\cos\theta)\,\hat{z}. \qquad (6.1.29)$$

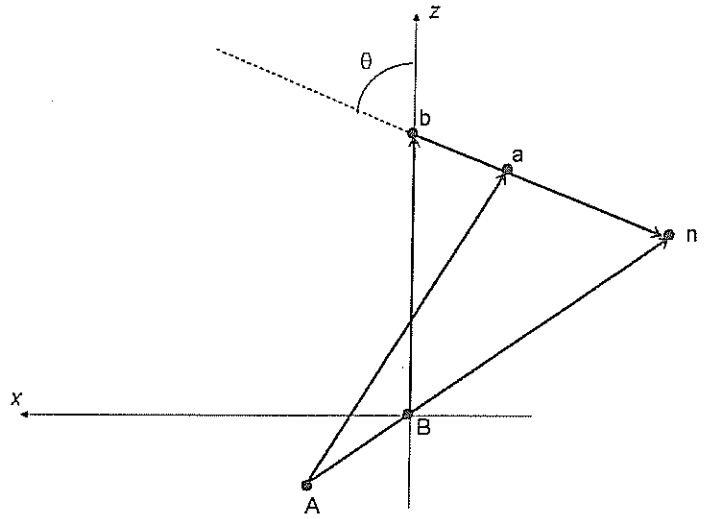

Figure 6.1.2: Coordinate system in the "standard" configuration. Note that $\mathbf{r}_f \equiv \mathbf{r}_{Bb}$, and $\mathbf{r}_i \equiv \mathbf{r}_{Aa}$.

One can then write

$$\mathbf{r}_{An} = \frac{A+1}{A}\mathbf{r}_{Bn} = -\frac{A+1}{A} r_{bn} \sin\theta\,\hat{x} + \frac{A+1}{A}(r_f - r_{bn}\cos\theta)\,\hat{z}, \tag{6.1.30}$$

$$\mathbf{r}_{an} = \frac{b}{b+1}\mathbf{r}_{bn} = -\frac{b}{b+1} r_{bn}(\sin\theta\,\hat{x} + \cos\theta\,\hat{z}), \tag{6.1.31}$$

and

$$\mathbf{r}_i = \mathbf{r}_{An} - \mathbf{r}_{an} = -\frac{2A+1}{(A+1)A} r_{bn}\sin\theta\,\hat{x} + \left(\frac{A+1}{A} r_f - \frac{2A+1}{(A+1)A} r_{bn}\cos\theta\right)\hat{z}, \tag{6.1.32}$$

where A, b are the number of nucleons of nuclei A and b respectively.

please correct

6.1.2 Zero–range approximation

In the zero range approximation,

$$\int dr_{bn} r_{bn}^2 u_{j_i}(r_{bn}) V(r_{bn}) = D_0; \quad u_{j_i}(r_{bn}) V(r_{bn}) = \delta(r_{bn})/r_{bn}^2. \tag{6.1.33}$$

6.1.2

It can be shown (see Fig. 7.1) that for $r_{bn} = 0$

$$\mathbf{r}_{An} = \frac{m_A+1}{m_A}\mathbf{r}_f, \quad \mathbf{r}_i = \frac{m_A+1}{m_A}\mathbf{r}_f \tag{6.1.34}$$

One then obtains

$$t_{ll'}^K = \frac{-16\sqrt{2}\pi^2}{k_f k_i}(-1)^K \frac{D_0}{\alpha} i^{l'-l} e^{\sigma_f^l + \sigma_i^{l'}} \frac{\sqrt{(2l+1)(2l'+1)(2l_i+1)(2l_f+1)}}{2K+1} ((l_f \tfrac{1}{2})_{j_f}(l_i \tfrac{1}{2})_{j_i} | (l_f l_i)_K (\tfrac{1}{2}\tfrac{1}{2})_0)_K$$
$$\times \langle l\, l'\, 0\, 0 | K\, 0\rangle \langle l_f\, l_i\, 0\, 0 | K\, 0\rangle \int dr_f\, f_l(r_f) g_{l'}(\alpha r_f) u_{j_f}(\alpha r_f), \tag{6.1.35}$$

with

$$\alpha = \frac{A+1}{A}. \tag{6.1.36}$$

6.2 Examples and Applications

In this section we discuss some examples which illustrate the workings of single–particle transfer processes at large, and in particular the flavour of the limitations by which nuclear structure studies suffer, when this specific probe to study quasiparticle properties is not operative. Let us in fact start with such an example.

6.2.1 Dressing of single–particle states: parity inversion in ^{11}Li

The $N = 6$ isotope of $^{9}_{3}$Li displays quite ordinary structural properties and can, at first glance, be thought of a two-neutron hole system in the $N = 8$ closed shell. That this is not the case emerges clearly from the fact that ^{10}Li is not bound, the lowest virtual $(1/2^+)$ and resonant $(1/2^-)$ states, testify to the fact that, in the present case, the $N = 6$ is a far better magic neutron number than $N = 8$. Furthermore, that the unbound $s_{1/2}$ state lies lower than the unbound $p_{1/2}$ state in plain contradiction with static mean field theory. Dressing the (standard) mean field single-particle states with vibrations, mostly with the core quadrupole vibration, through polarization (effective mass like) and correlation diagrams (vacuum zero point fluctuations (ZPF)) diagrams, similar to those associated with the (lowest order) Lamb shift Feynman diagrams (cf. App 6.C), move the $s_{1/2}$ and $p_{1/2}$ mean field levels around. In particular the $p_{1/2}$ from a bound state (≈ -1.2MeV) to a resonant state lying at ≈ 0.5 MeV (Pauli principle, vacuum ZPF process), the $s_{1/2}$ being lowered and becoming a virtual state (≈ 0.2 MeV).

How can one check that CO and PO like processes as the ones shown in Fig. 6.1.3 (I) (cf. also Fig. 6.D.1) are the basic processes dressing the odd neutron of ^{10}Li, and thus the mechanism at the basis of parity inversion? The answer is, forcing these virtual processes to become real. While this is not easy to accomplish in one–particle transfer processes involving the unbound $s_{1/2}$ and $p_{1/2}$, ^{10}Li virtual and resonant states respectively, it can be done with the help of two–particle transfer processes, namely that associated with inverse kinematics (p, t) reaction ^{1}H(^{11}Li,^{9} Li(2.69MeV; $1/2^-$))^{3}H (cf. Fig. 6.V.1 and Eqs. 7.2.10 and 8.2.3). Such a reaction is feasible and has been studied (I. Tanihata et al., 2008), in keeping with the fact that, adding a neutron to ^{10}Li leads to a bound state (see Fig. 6.1.3 (II)). In fact, $^{11}_{3}$Li$_8$ displays a two–neutron separation energy $S_{2n} \neq 400$ keV (for further details we refer to Ch. 8, Sect. 8.2). A price to pay for not being able to use the specific probe for single–particle modes (one–particle transfer), is that of adding to the self–energy contributions in question those corresponding to vertex corrections (for details cf. App 6.D, Figs 6.D.1 and 6.D.2 and Ch. 8.2.3 Sect. 8.2 (application $2n$–transfer)). Within the present context, it is difficult if not impossible to talk about single–particle motion without also referring to collective vibrational states (cf. e.g. Fig. 6.1.3 (II)) to talk about pair addition and pair substraction correlations, without at the same time talking about vibrations and dressed quasiparticle motion (see e.g. Fig. 6.1.4 (a) and (b)), again concerning both structure and reactions. Within the framework of the present monograph, the above facts imply that Chapters 5 (inelastic), 6.2.1 (one–particle transfer) 7.2.10 and 8.2.3 (two–particle transfer and applications) form a higher unity. This unity extends also

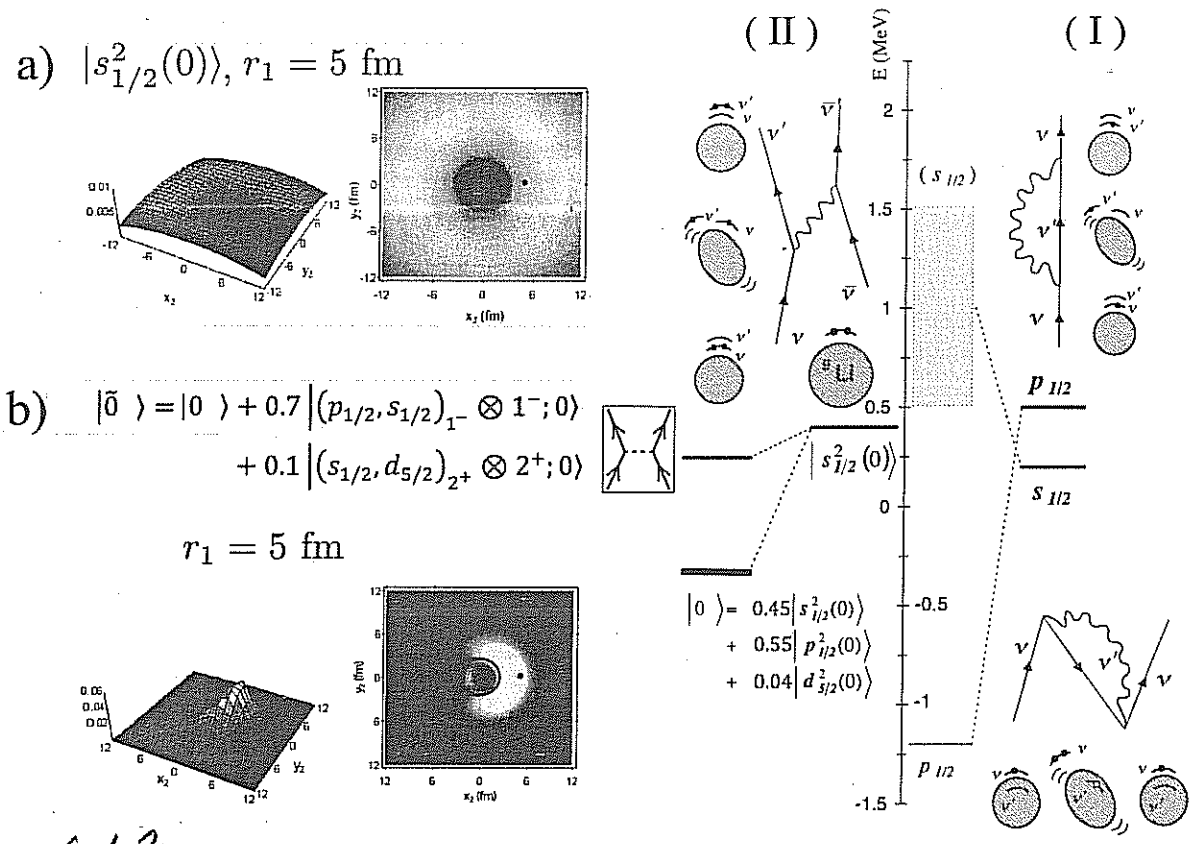

6.1.3 NFT

Figure 6. *The NFT scheme synthetized in Figs. 1a)-f) and Fig. 4a)-c) becomes operative concerning the structure of ^{10}Li and ^{11}Li: (I) self-energy processes, giving rise to parity inversion in ^{10}Li; (II) bare (boxed inset) and induced pairing interaction binding the halo neutron pair to the ^{9}Li core, through a bootstrap mechanism, in which the neutrons exchange the pigmy dipole resonance of ^{11}Li, as well as the quadrupole vibration of the core, as testified by the wavefunction b).*

In other words, the color snapshots displayed in a) and b) attempt at describing the becoming of the neutron halo Cooper pair of ^{11}Li, from an uncorrelated $s^2_{1/2}(0)$ configuration to a strongly correlated, (weakly) bound two-neutron state. It is of notice that the bare interaction (boxed inset in (II)), corresponding to the process depicted in Fig. 1d) (NFT four-point vertex, rule (II) of NFT, cf. e.g. ref. [55], p. 314) lowers the $s^2_{1/2}(0)$ (as well as the $p^2_{1/2}(0)$) pure configurations by only 100 keV, and is not able, by itself, to bind the pair. The color plots display the modulus square of the two-neutron wavefunction as a function of the coordinates of the two nucleons (left) and the probability distribution of one neutron with respect to the second one held fixed on the x-axis (at a radius of 5fm, solid dot). The red circle schematically represents the core. After [55].

8He

Barrosco et al (2001)

Nev Rec

The renormalization processes in which the neutrons of the halo Cooper pair of ^{11}Li either emit and reabsorb a collective (p-h)-like quadrupole vibration (effective mass processes, Fig. 1e)) or exchange a phonon (vertex correction, Fig. 1f)) can, in a two-particle pick-up reaction (Fig. 1g)), populate the first excited state , lowest energy (E^* = 2.69 MeV) member of the multiplet of ^{9}Li. The absolute value of the corresponding two-nucleon transfer cross section provides an accurate measure of the probability with which the component appears in the ^{11}Li ground state (cf. Fig 6b)) and thus of the role the quadrupole vibration plays in binding the neutron halo Cooper pair. This is also in keeping with the fact that alternative channels, like final-state inelastic excitation and neutron break-up, lead to negligible contributions [24].

The fact that theory reproduces the observed absolute differential cross sections, testifies to the fact that *NFT* of structure and reactions [39,54,55], is able to accurately predict [58] and describe [24] the consequences of the induced nuclear pairing interaction.

While this result can, arguably, be considered a milestone in the understanding of the origin of pairing in nuclei, we feel equally important and timely the developments taking place at a breathtaking pace,

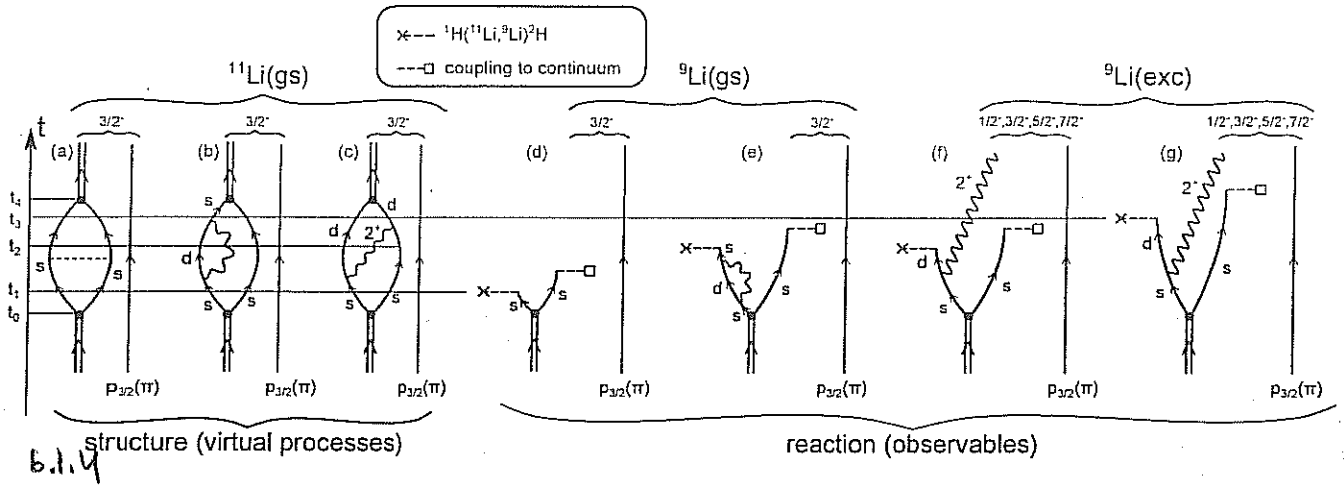

6.1.4

FIG. 1: Nuclear Field Theory diagrams describing the basic, lowest order processes, by which the di–neutron halo binds to the $^9_3\mathrm{Li}_6$ core (**structure**), and those associated with a one–neutron pick–up process like e.g. (p,d) (**reaction**). In keeping with the fact that ^{10}Li is not bound, such a reaction populates only transiently the virtual and resonant states of ^{10}Li and eventually, after the second neutron of the pair spoliated of its dynamical glue leaves the system by going into the continuum, a state in ^{9}Li is populated. In drawing the different NFT diagrams time t is assumend to run upwards. External fields and the bare NN–interaction are assumed to act instantaneously, while the couplings to the phonon modes (wavy lines) lead to retarded (ω–dependent) effects. For simplicity, only the quadrupole vibrate of the ^{8}He core is considered, as well as only the virtual s– and continuum d– single–particle states are considered. The halo Cooper pair (pair addition mode of the $N = 6$ closed shell system) carries angular momentum 0^+ and is represented by a double arrowed line, the odd proton (π) which occupies a $p_{3/2}$ state, represented by a single arrowed being a spectator. The di–neutron system binds to the core through (a) the bare interaction (horizontal dashed line) acting between the two–neutron, each represented by a single arrowed line; (b) effective mass processes associated with the quadrupole vibration of ^{8}He (wavy line) renormalizing the energy of the $s_{1/2}$ continuum state and leading to an almost bound (virtual) state (≈ 0.2 MeV). (c) Induced pairing interaction associated with the quadrupole vibration of ^{8}He. (d) Intervening the process (a) at any time after to and before t_4 with an external single–neutron pick–up field and processes (b) and (c) at $t_0 < t < t_1$, in particular with the (^{1}H,^{2}H) field (cross followed horizontal dashed line), leads to the ground state of ^{9}Li, in keeping with the fact that the second neutron will leave the system almost immediately, ^{10}Li not being stable. (e) Same as above but in connection with process (b) and now after the nucleon has reabsorbed the quadrupole phonon and before t_4, i.e. acting at $t_3 < t < t_4$ leads again to the population of the ^{9}Li ground state. Let us now consider the one–nucleon transfer processes populating the $(2 \otimes p_{3/2}(\pi))_{J^\pi}(J^\pi = 1/2^-, 3/2^-, 5/2^-\text{and}\, 7/2^-)$ multiplet of ^{9}Li, in particular the lowest $|1/2^-; 2.69\,\mathrm{MeV}\rangle$ state. (f) Same as above, that is in connection with process (b), but before the phonon is reabsorbed. (g) Same as above but in connection with process (c), and acting at any time after the phonon has been emitted and before it is reabsorbed ($t_1 < t < t_2$). While the single contribution associated with mass renormalization process ((b)→ (f)) and vertex corrections ((c)→ (g)) cannot be experimentally distinguished, one can estimate the relative contribution to the corresponding absolute cross section. The wavefunction of ref. [?] (cf. also Fig. ?? (b)) predict a ratio 3/1.

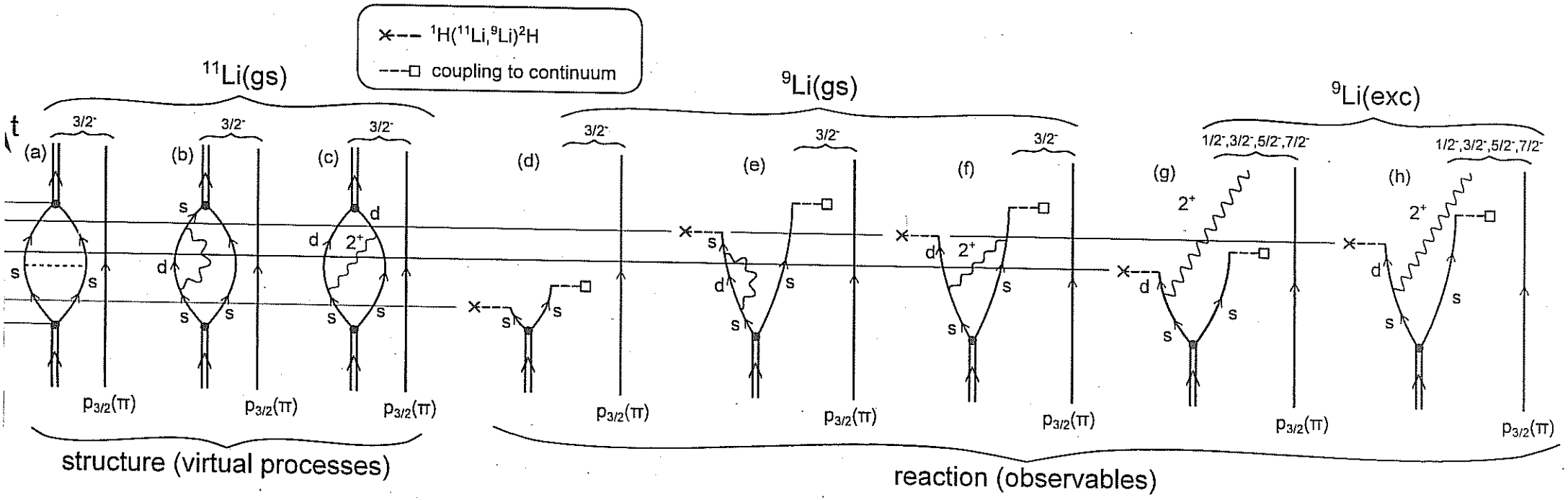
^{1}H(^{11}Li,^{9}Li)^{2}H
coupling to continuum
^{11}Li(gs)
^{9}Li(gs)
^{9}Li(exc)
(a)
(b)
(c)
(d)
(e)
(f)
(g)
(h)
3/2$^-$
1/2$^-$,3/2$^-$,5/2$^-$,7/2$^-$
2$^+$
s
d
p$_{3/2}$(π)
structure (virtual processes)
reaction (observables)

Eventually bring this Fig. to Ch. 8, but only at the end, when the book is structured.

do not mix things

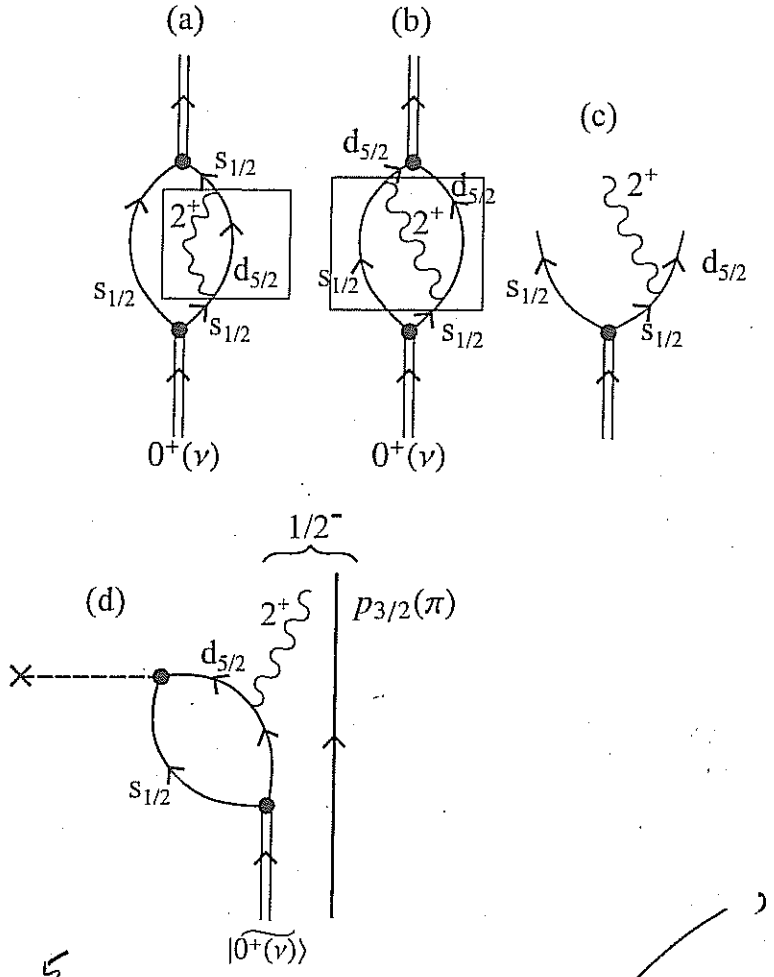

Figure 6.1: (a)Self–energy (see boxed process) and (b) vertex (pairing induced interaction) ~~boxed process~~) renormalization process, both associate with (c) a (two–particle)–(quadrupole vibration) intermediate (virtual state) which can be forced to became real in a (p,t) reaction ^{1}H(^{11}Li,^{9}Li)^{3}H exciting the first excited state $|$~~12.69~~MeV;$1/2^-\rangle$ of ^{9}Li (see Ch.8.2.3).

1.69

write please

6.2.2 $^{132}Sn(d,p)^{133}Sn$ and $^{132}Sn(p,d)^{131}Sn$ reactions

6.2.3 $^{120}Sn(d,p)^{121}Sn$ and $^{120}Sn(p,d)^{119}Sn$ reactions

drawing Front

PRL all multi step proton (ch. 8)

to the content of App. 6.F (knock–out reactions), if one also considers the question of final state interactions, and thus of the possibility that the population of the excited state $1/2^-$ depicted in Fig. 6.1.4 (d) receives contributions other, and more involved, than those associated with the direct two–nucleon pick–up depicted (for details cf. Ch. 8.2.3; cf. also (Potel et al., 2010)).

Figs. 6.1.4(g) and (h) and of

Appendix 6.A Minimal requirements for a consistent mean field theory

In what follows the question of why, rigorously speaking, one cannot talk about single–particle motion, let alone spectroscopic factor, not even within the framework of Hartree–Fock theory, is briefly touched upon.

As can be seen from Fig. 6.A.1 the minimum requirements of selfconsistency to be imposed upon single–particle motion requires both non–locality in space (HF) and in time (TDHF)

$$i\hbar\frac{\partial\varphi_\nu}{\partial t} = -\frac{\hbar^2}{2m}\nabla^2\varphi_\nu(x,t) + \int dx'dt' U(x-x',t-t')\varphi_\nu(x',t'), \tag{6.A.1}$$

and consequently also of collective vibrations and, consequently, from their interweaving to dressed single–particles (quasiparticles), let alone renormalized collective modes. Assuming for simplicity infinite nuclear matter (confined by a constant potential of depth V_0), and thus plane wave solutions, the above time–dependent Schrödinger equation leads to the quasiparticle dispersion relation (cf. e.g. Brink and Broglia (2005))

$$\hbar\omega = \frac{\hbar^2k^2}{2m^*} + \frac{m}{m^*}V_0, \tag{6.A.2}$$

where the effective mass

$$m^* = \frac{m_k m_\omega}{m}, \tag{6.A.3}$$

in the product of the k–mass

$$m_k = m\left(1 + \frac{m}{\hbar^2 k}\frac{\partial U}{\partial k}\right)^{-1}, \tag{6.A.4}$$

closely connected with the Pauli principle $\left(\frac{\partial U}{\partial k} \approx \frac{\partial U_x}{\partial k}\right)$, while the ω–mass

$$m_\omega = m\left(1 - \frac{\partial U}{\partial\hbar\omega}\right), \tag{6.A.5}$$

results from the dressing of the nucleon through the coupling with the (quasi) bosons. Because typically $m_k \approx 0.7m$ and $m_\omega \approx 1.4m$ $m^* \approx m$, one could be tempted to conclude that the results embodied in the dispersion relation (6.A.2) reflects that the distribution of levels around the Fermi energy can be described in terms of the solutions of a Schrödinger equation in which nucleons of mass equal to the bare nucleon mass m move in a Saxon–Woods potential of depth V_0.

Now, it can be shown that the occupancy of levels around ε_F is given by Z_ω (cf. Fig. 6.A.1 (h)) a quantity which is equal to $m/m_\omega \approx 0.7$. This, in keeping with the fact that the time the nucleon is coupled to the vibrations it cannot behave as a single–particle and can thus not contribute to e.g. the single–particle pickup cross section.

lettere più grandi sia testo che equazioni, e.g U_x is hardly visible

, the discontinuity at the Fermi energy

(d') $U_x(r,r') = -\sum_{i(\varepsilon_i \le \varepsilon_F} \varphi_i^*(\vec{r}') v(|\vec{r}-\vec{r}'|) \varphi_i(\vec{r})$

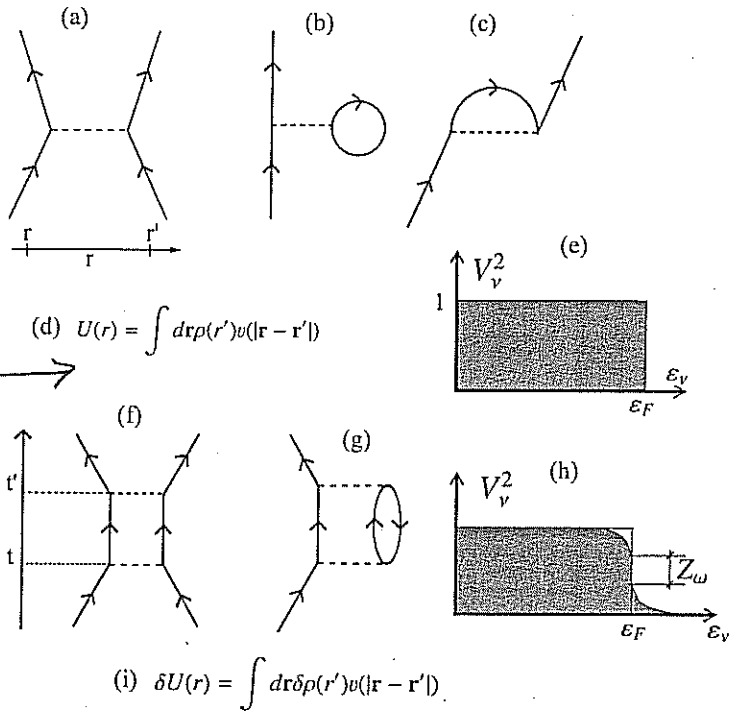

Figure 6.A.1: (a)Scattering of two nucleons through the bare *NN* interaction $v|\mathbf{r}-\mathbf{r}'|$, (b) contribution to the direct (U, Hartree) and (c) to the exchange (U_x, Fock) potential, resulting in (d) the (static) self–consistent relation between potential and density (non–local (d')), which (e) uncouples occupied ($\varepsilon_\nu \le \varepsilon_F$) from empty states ($\varepsilon_\nu > \varepsilon_F$), (f) multiple scattering of two nucleons lead, through processes like the one depicted in (g), eventually propagated to all orders, to: (h) softening of the discontinuity of the occupancy of levels at ε_F, as well as to: (i) generalization of the static selfconsistency into a dynamic relation encompassing also collective vibrations (Time–dependent HF solutions of the nuclear Hamiltonian, conserving energy weighted sum rules (EWSR).

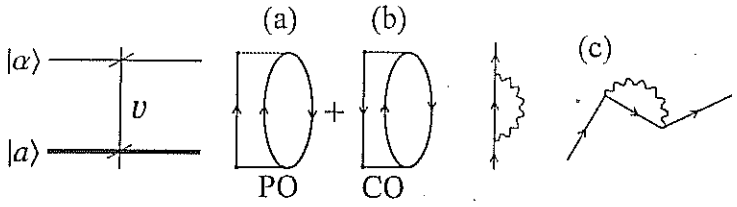

Figure 6.B.1: Two state schematic model describing the breaking of the strength of the pure single–particle state $|a\rangle$, through the coupling to collective vibrations (wavy line) associated with polarization (PO) and correlation (CO) processes.

It is of notice that the selfconsistence requirements for the iterative solution of Eq. 6.A.1 (see Fig. 6.A.1 (d) and (d')) remind very much those associated with the solution of the Kohn–Sham equations

$$H^{KS}\varphi_\gamma(\mathbf{r}) = \lambda_\gamma\varphi_\gamma(\mathbf{r}), \tag{6.A.6}$$

where

$$H^{KS} = -\frac{\hbar^2}{2m_e}\nabla^2 + U_H(\mathbf{r}) + V_{ext}(\mathbf{r}) + U_{xc}(\mathbf{r}), \tag{6.A.7}$$

H^{KS} being known as the Kohn–Sham Hamiltonian, $V_{ext}(\mathbf{r})$ being the field created by the ions and acting on the electrons. Both the Hartree and the exchange–correlation potentials $U_H(\mathbf{r})$ and $U_{xc}(\mathbf{r})$ depend on the (local) density, hence on the whole set of wavefunctions $\varphi_\gamma(\mathbf{r})$. Thus, the set of KS–equations must be solved selfconsistently (cf. e.g. (~~Broglia and Winther, 2004~~) and refs. therein).

(Broglia, Colò, Onida et al, 2004)

Appendix 6.B Model for single–particle strength function: Dyson equation

concerning

In the previous section we introduce the argument of the impossibility of defining a "bona fide" single–particle spectroscopic factor. It was done with the help of Feynman (NFT) diagrams. In what follows we essentially repeat the arguments, but this time in terms of Dyson's (Schwinger) language. For simplicity, we consider a two–level model where the pure single–particle state $|a\rangle$ couples to a more complicated state $|\alpha\rangle$, made out of a fermion (particle or hole), couple to a particle–hole excitation which, if iterated to all orders can give rise to a collective state (cf. Fig. 6.B.1). The Hamiltonian describing the system is

$$H = H_0 + v \tag{6.B.1}$$

where

$$H_0|a\rangle = E_a|a\rangle, \tag{6.B.2}$$

and

$$H_0|\alpha\rangle = E_\alpha|\alpha\rangle. \tag{6.B.3}$$

Let us call $\langle a|v|\alpha\rangle = v_{a\alpha}$ and assume $\langle a|v|a\rangle = \langle\alpha|v|\alpha\rangle = 0$.

From the secular equation

$$\begin{pmatrix} E_\alpha & v_{a\alpha} \\ v_{a\alpha} & E_a - E_i \end{pmatrix}\begin{pmatrix} C_\alpha(i) \\ C_a(i) \end{pmatrix} = 0, \tag{6.B.4}$$

and associated normalization condition

$$C_a^2(i) + C_\alpha^2(i) = 0, \tag{6.B.5}$$

one obtains

$$C_a^2(i) = \left(1 + \frac{v_{a\alpha}^2}{(E_a - E_i)^2}\right)^{-1}, \tag{6.B.6}$$

and

$$\Delta E_a(E) = E_a - E = \frac{v_{a\alpha}^2}{E_a - E}. \tag{6.B.7}$$

The energy of the correlated state

$$|\tilde{a}\rangle = C_a(i)|a\rangle + C_\alpha(i)|\alpha\rangle, \tag{6.B.8}$$

is obtained by the (iterative) solution of the Dyson equation (6.B.7), which propagate the bubble diagrams shown in Figs 6.B.1 (a) and (b) to infinite order leading to collective vibrations (see Fig. 6.B.1 (c))

With the help of the definition given in Eq. (6.B.5) and making use of the fact that in the present case, $U \equiv \Delta E_a(E)$, one obtains

$$Z_\omega = C_a^2(i) = \left(\frac{m_\omega}{m}\right)^{-1}. \tag{6.B.9}$$

Making use of the solution of the Dyson equation (6.B.7), and of the relations (6.B.5) and (6.B.6), one can calculate the renormalized state $|\tilde{a}\rangle$, to be employed in working out the associated modified, single–particle transfer form factor.

Appendix 6.C The Lamb Shift

In Fig. 6.C.1 we display a schematic summary of the electron–photon processes, associated with Pauli principle corrections, leading to the splitting of the lowest s, p states of the hydrogen atom known as the Lamb shift.

In the upper part of the figure the predicted position of the electronic single–particle levels of the hydrogen atom as resulting from the solution of the Schrödinger equation (Coulomb field). In the lowest part of the figure one displays the electron of an hydrogen atom (upwards going arrowed line) in presence of vacuum ZPF (electron–positron pair plus photon, oyster–like diagram). Because the associate electron virtually occupies states already occupied by the hydrogen's electron, thus violating Pauli principle, one has to antisymmetrize the corresponding two–electron state. Such process gives rise to the exchange of the corresponding fermionic lines and thus to CO–like diagrams as well as, through time ordering, to PO–like diagrams. The results provide a quantitative account of the experimental findings.

Appendix 6.D Self–energy and vertex corrections

In Fig. 6.D.1 an example of the fact that in field theories (e.g. QED or NFT), nothing is really free and that e.g., the bare mass of a fermion (electron or nucleon), is the parameter one adjusts (m_k) so that the result of a measurement (cf. Fig. 6.D.1) gives the observed mass (single particle energy). In Fig. 6.D.2, lowest order diagrams associated with the renormalization of the fermion–boson interaction (vertex corrections)